Chinese Chemical Letters 33 (2022) 3073–3077

Contents lists available at ScienceDirect

Chinese Chemical Letters

journal homepage: www.elsevier.com/locate/cclet

Engineering FeS_2 nanoparticles on tubular g-C_3N_4 for photo-Fenton treatment of paint wastewater

Chan Wang*, Bangqi Wei, Han Zhu, Yimin He, Guoxia Ran, Qijun Song*

Key Laboratory of Synthetic and Biological Colloids, Ministry of Education, International Joint Research Center for Photoresponsive Molecules and Materials, School of Chemical & Material Engineering, Jiangnan University, Wuxi 214122, China

ARTICLE INFO

Article history:
Received 24 May 2021
Revised 18 August 2021
Accepted 14 September 2021
Available online 20 September 2021

Keywords:
Photo-Fenton catalysts
FeS_2 nanoparticles
Hollow tubular g-C_3N_4
Heterojunction
Reactive oxygen species
Paint wastewater degradation

ABSTRACT

An efficient photo-Fenton catalyst (FeS_2@HTCN) was designed by maximizing the synergistic effect of FeS_2 nanoparticles and hollow tubular g-C_3N_4 (HTCN). Molecule self-assembly and molten salts-assisted calcination were used to engineering the hollow structured g-C_3N_4 before anchoring FeS_2 nanoparticles on the walls of HTCN via reflux method. Compared to bulk g-C_3N_4, the unique structure of HTCN and heterojunction in the composite endowed FeS_2@HTCN with more active sites and abundant channels for electron transfer and charge separation. The enriched electrons can improve the Fe^{3+} recycling and boost Fe^{2+} catalyzed $^{\bullet}OH$ production *via* H_2O_2. As-prepared photo-Fenton catalyst was successfully applied to the treatment of industrial paint wastewater. The paint wastewater with its COD as high as 8200 mg/L can be effectively degraded with 0.2 mol/L H_2O_2 in 90 min under visible light irradiation. The photo-Fenton system was further evaluated according to the process stability and economic benefit, proving that the strategy presented in this work would be applicable to the treatment of real wastewater.

With the increase in vehicle production, a large quantity of wastewater is generated during the process of painting and coating in paint workshop section [1–3], which evoked increased environment concerns. Paint wastewaters contain suspended waste paint and organic additives, making them present high turbidity, chemical oxygen demand (COD) and toxicity [4–6]. Treatment of such waters to achieve permissible discharge level is still a great challenge. Advanced oxidation processes (AOPs) are considered as the cost-effective method for heavily polluted waters [7–9]. Owing to the broad applicability, relatively cheap reagents and environmental friendliness, Fenton type processes are the widely used AOPs, in which the highly reactive oxygen species (ROS) are generated with homogeneous Fe^{2+} and H_2O_2. The hydroxyl radicals ($^{\bullet}OH$), as one of the major ROS, possess stronger oxidation capability than the pristine oxidants (such as O_2 and H_2O_2). And it was found that the currently applied AOPs with the assistant of ultraviolet light irradiation, in a reaction that is called the "photo-Fenton technology", could increase the number of $^{\bullet}OH$, enhance the reduction of Fe^{3+} to Fe^{2+} and thus improve the Fenton oxidation efficiency [10–14]. However, the homogeneous reactions suffer from several drawbacks in practical applications, such as the requirement of high dosage reagents, energy usage for ultraviolet light, narrow pH range, and production of a large amount of iron sludgy [15,16]. Consequently, such photo-Fenton process is not ideal for the treatment of paint wastewaters.

Intensive research efforts are devoted to develop heterogeneous photo-Fenton reactions that use insoluble iron-based solid catalyst instead of soluble iron salts [17,18]. Composite photocatalysts by coupling iron species with foreign materials through heterojunction are widely utilized to improve the catalyst efficiency. In this regard, titanium dioxide [19,20], graphene [21,22], graphitic carbon nitride (g-C_3N_4) [23–25] were employed to provide abundant active sites, and promote the separation and transfer of photo-generated electron-hole ($e^- - h^+$) pairs. Our group also reported a FeS_2@g-C_3N_4 hybrid for pollutants degradation under visible light irradiation [26]. However, the photocatalysts reported so-far are still not efficient enough, as the degradation of pollutants at about 6000 mg/L level usually takes several hours to complete approximately 70%–80% [21,22]. Furthermore, most of above studies are limited to the treatment of simulated wastewaters, which are significantly different from real industrial ones [10,27,28].

In this study, a structural engineering strategy is used to further improve the photocatalytic performance of catalyst. Hollow tubular g-C_3N_4 (HTCN) with augmented contact area was fabricated, and then FeS_2 nanoparticles were immobilized on the wall of HTCN *via* the heterojunction formation. The resulting FeS_2@HTCN exhibited

* Corresponding authors.
E-mail addresses: wangchan@jiangnan.edu.cn (C. Wang), qsong@jiangnan.edu.cn (Q. Song).

https://doi.org/10.1016/j.cclet.2021.09.051
1001-8417/

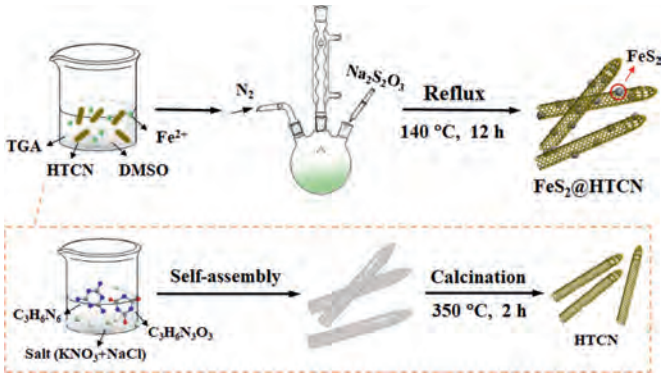

Scheme 1. The schematic illustration of FeS_2@HTCN formation.

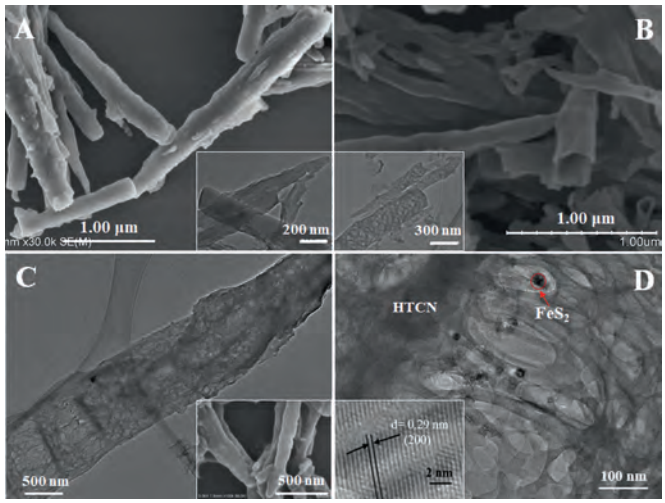

Fig. 1. SEM images of melamine-cyanuric acid complexes (A) and HTCN (B). Inset: TEM images. (C) and (D) TEM images of $(FeS_2)_{0.15}$@HTCN. Inset: SEM image and HRTEM image.

an enhanced light absorption and migration efficiency of charge carriers, leading to the improved Fe^{2+}/Fe^{3+} cycling and $^{\bullet}OH$ generation. Thus a substantially enhanced degradation efficiency was obtained for the treatment of heavily polluted waters. The operating costs, sludge production, process stability, and the reusability of the catalyst are also superior than other reported Fenton processes for real paint wastewater treatment.

Scheme 1 schematically illustrates the preparation procedures of FeS_2@HTCN. First, the supramolecular complexes were obtained by the hydrogen bonds orientated self-assembling of melamine and cyanuric acid [29–31]. Then the HTCN was synthesized by the molten salt method after the optimization of reaction parameters (Figs. S1−S4 in Supporting information). The formation of tubular structure is attributed to the high-temperature liquid media of molten salts, and fine tuning of calcination temperature and time [32]. Finally, the FeS_2 nanoparticles were generated and anchored on the wall of HTCN. As shown in Fig. S5A (Supporting information), the addition of 15 wt% FeS_2 in the composite ($(FeS_2)_{0.15}$@HTCN) was found to have the highest COD removal rate of 90%, whereas only 8.5% could be reduced in the present of only g-C_3N_4. The enormous increase in degradation rate may be attributed to high specific surface area of HTCN and the introduction of the FeS_2 heterojunction. N_2 adsorption results indicate that the involvement of FeS_2 has almost no impact on the surface area of HTCN (Fig. S5B in Supporting information). And Fig. S5C (Supporting information) shows that the zeta potentials of FeS_2 and HTCN are respectively +11.88 and −35.15 mV, and the FeS_2@HTCN composites are formed through electrostatic interaction. The peaks at 27.4° in the XRD spectra (Figs. S5D and E in Supporting information) can be attributed to the conjugated aromatic segments in HTCN (JCPDS No. 87-1526). Note that a slight right-shift of this peak toward the characteristic peak of (111) FeS_2 implies a decreased interplanar spacing of HTCN and the existence of interfacial interaction between FeS_2 and HTCN [33–36]. Besides, the distinct bands at about 2180 cm^{-1} in FT-IR spectra (Fig. S5F in Supporting information) indicate the presence of terminal cyano group (−CN) in both HTCN and $(FeS_2)_{0.15}$@HTCN [37,38]. Their intensities become weakened after the introduction of FeS_2, suggesting the formation of chemical bond (such as Fe−N) between FeS_2 and HTCN. XPS spectra (Fig. S6 in Supporting information) exhibit that a new peak at around 286.5 eV in C 1s spectra ascribed to −CN group can be observed in HTCN, and its signal is intensified in $(FeS_2)_{0.15}$@HTCN. And the peak of the C–N−H group in N 1s spectra is broadened and right-shifted, indicating the formation of the N−Fe bonds [17]. These results prove that the heterojunction structure was successfully formed in FeS_2@HTCN.

The morphologies of the supramolecular complexes, HTCN and $(FeS_2)_{0.15}$@HTCN are presented in Fig. 1. A rod-like structure about several microns in length was observed for melamine-cyanuric acid complexes (Fig. 1A). After pyrolysis in the salt matrix, the open-ended tubes were obtained (Fig. 1B), and the corresponding TEM image shows the abundant pores formed on the wall of these tubes (Fig. 1C). The black FeS_2 nanoparticles are decorated on the surface of HTCN and the lattice spacing of 0.29 nm is slightly larger than that of common FeS_2 phase (0.27 nm) (Fig. 1D), presumably due to the formation of Fe−N bonds with HTCN [37,38]. The photoelectric properties of HTCN and FeS_2@HTCN composites were further investigated. UV–vis DRS results presented in Fig. S7A (Supporting information) exhibit that the HTCN possesses UV to visible light absorbance with an absorption edge at about 420 nm, while the FeS_2@HTCN composites has an enhanced absorption in visible-light region, which is favorable for visible-light-driven photocatalysis. In addition, the semicircle arc radius of $(FeS_2)_{0.15}$@HTCN in EIS Nyquist plot is smaller than other catalysts (Fig. S7B in Supporting information), and these results confirm that $(FeS_2)_{0.15}$@HTCN has a low interfacial charge transfer resistance and high transport efficiency. In the PL spectra (Fig. S7C in Supporting information), the emission intensities of the composites gradually decrease with the increase of FeS_2, indicating that the e^-−h^+ pairs recombination rate is decreased with the increase of FeS_2 content. The time-resolved PL decay spectra also verified the above results (Fig. S7D and Table S1 in Supporting information). The PL lifetimes of all FeS_2@HTCN composites are longer than that of HTCN indicating that the formation of FeS_2 heterojunction on HTCN can promote migration and separation rate of charge carries.

It is noted that model pollutants may be transformed to other intermediates rather than degraded, hence monitoring the concentration of pollutants cannot properly reflect the degradation efficiency, and the reduction in COD value is more meaningful in practical applications. Batch photo-Fenton experiments were conducted to determine the optimum operating conditions (Fig. 2). The adsorption effect to potassium biphthalate (KHP) is relatively weak over the $(FeS_2)_{0.15}$@HTCN within 30 min under dark conditions. After irradiating by visible light, COD reduction is intensified, and the removal rates increase up to nearly 100% after 90 min irradiation. The effect of H_2O_2 concentration on the degradation performance was investigated (Fig. 2B). The removal rates increase from 16.1% to 98.8% with the increase of H_2O_2 concentration up to 0.2 mol/L, then no further promotion in the degradation rates were observed, presumably because the excess H_2O_2 would lead to the $^{\bullet}OH$ consumption (*i.e.*, $H_2O_2 + {}^{\bullet}OH \rightarrow {}^{\bullet}O_2H + H_2O$) [39,40], and the interference in COD test by the excessive consumption of ox-

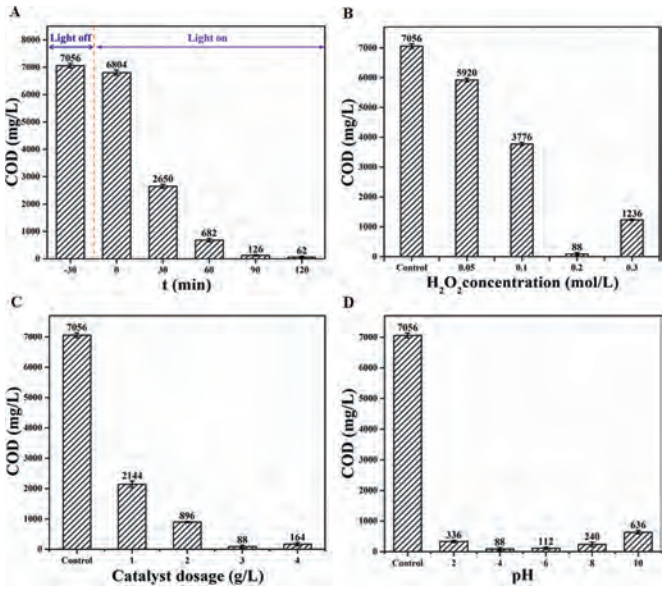

Fig. 2. Optimization of degradation conditions in $(FeS_2)_{0.15}$@HTCN/H_2O_2/vis system. Effect of degradation time (A), H_2O_2 concentration (B), catalyst dosage (C), and pH value (D).

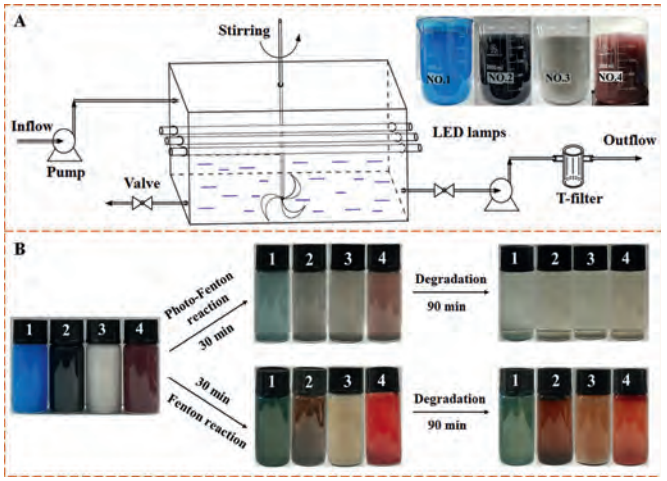

Fig. 3. (A) Schematic illustration of degradation process of painting wastewater in the self-made reactor, and (B) comparison between Fenton and photo-Fenton degradation process.

idant. The effect trend of catalyst dosage on the degradation of KHP is same as that of H_2O_2 concentration (Fig. 2C). Once catalyst dosage exceeded the 3 g/L, the increase in $(FeS_2)_{0.15}$@HTCN amount do not affect the removal rate. As shown in Fig. 2D, the $(FeS_2)_{0.15}$@HTCN/H_2O_2/vis system exhibits a good adaptability in a wider pH range with more than 90% of removal rate. The pH variation of KHP solution was also monitored (Fig. S8 in Supporting information). According to the above experiments, the subsequent experiments are conducted in the present of 3.0 g/L catalyst and 0.2 mol/L H_2O_2 under 90 min irradiation.

The degradation experiments were conducted in a self-made reactor (Fig. 3A), of which picture and operational process were illustrated in Fig. S9 (Supporting information). Four paint effluents (2 L) with COD values in the range of 5500−8200 mg/L were investigated and labelled as No. 1, 2, 3 and 4, respectively. The color of all samples gradually decreases with increase of time. After 90 min, the turbid water samples become clear (Fig. 3B). Compared with traditional Fenton reaction, our system showed a more effective degradation in same time interval. After treatment, the four effluents could meet the discharge standard of COD (Fig. S10 in Supporting information). Taking the No. 4 sample for example, only 5.87 g sediment was produced in our system, which is substantially less than the sludge (35.8 g) produced by a conventional Fenton method (Fig. S11A in Supporting information). The sediment contains used catalyst, which can be recycled with minimum loss of catalyst after a simple treatment (Fig. S11B in Supporting information). The morphology and composition of $(FeS_2)_{0.15}$@HTCN has not been changed after the durability tests (Figs. S11C and S11D in Supporting information). Recycle-experiment results (Fig. S12A in Supporting information) indicate that $(FeS_2)_{0.15}$@HTCN possesses high stability and little deactivation after four cycles. In addition, the concentration of Fe^{2+} and total Fe in different systems during 90 min irradiation were measured, and the results were shown in Fig. S12B (Supporting information). It is worthy to note that the concentration of dissolved Fe^{2+} and total Fe in FeS_2@HTCN/H_2O_2/vis system are much lower than those detected in the classic Fenton system [41], indicating the good stability of FeS_2@HTCN. And a lower ration of Fe^{2+} to total Fe in classic Fenton system means that a large amount of Fe^{2+} is transferred to Fe^{3+} and cannot be recycled during degradation. Total organic carbon (TOC) experiments were further investigated to demonstrate the degradation effectivity for No. 4 sample (Fig. S12C in Supporting information). Obviously, the total TOC removal rate can be up to 88.6% (90 min), suggesting a complete mineralization of paint wastewater could be achieved by simply increase the irradiation time. The degradation efficiency and overall cost of our system were compared with that of traditional Fenton in Table S2 (Supporting information), as can be seen that a huge improvement was achieved in degradation efficiency and running costs. In addition, the homogeneous photo-Fenton experiments were carried out for comparison purpose. As shown in Fig. S13 (Supporting information), 90.2% of COD removal rate can be observed after 120 min UV irradiation, and 0.32 g sediment is produced from every 50 mL wastewater. Owing to the relatively large amount of sludge and unreusable catalyst for homogeneous photo-Fenton system, the heterogeneous system exhibited a greater advantage. This observation agrees with the conclusion from the previous reported literatures [42,43]. A comparison with other technologies is also made in Table S3 (Supporting information). Obviously, our method exhibits short degradation time and high COD removal rate, which shows a promising application potential for the treatment of industrial wastewaters.

To explore the degradation mechanism, EPR experiments were carried out to identify the ROS species during the catalytic process. As shown in Figs. 4A and B, signal of $^{\bullet}OH$ was not detected in dark condition, while its characteristic signals were clearly observed in lightened condition without adding H_2O_2 or other materials than can produce $^{\bullet}OH$, indicating that the $^{\bullet}OH$ may be generated from the transition of other ROS (*i.e.*, $^{\bullet}O_2^-$). And the presence of $^{\bullet}O_2^-$ is not observed in EPR tests presumably due to its low concentration. Furthermore, both HTCN/H_2O_2/vis and $(FeS_2)_{0.15}$@HTCN/H_2O_2/vis systems displayed the enhanced signal of $^{\bullet}OH$ compared with the H_2O_2/vis system, and more $^{\bullet}OH$ is yielded in the present of FeS_2@HTCN-based photocatalytic process, confirming that the synergy (H_2O_2, catalyst and visible light) gives a boost to the generation of $^{\bullet}OH$ species. The control experiments (Fig. S14 in Supporting information) were explored to further elaborate the synergistic mechanism of photo-Fenton system for degradation of No. 4 sample. The degradation rate without FeS_2@HTCN is only 11.3%, suggesting the oxidizing capacity of H_2O_2 for degradation of organic pollutants is very weak under visible light irradiation. The degradation rate of 36.4% and 49.2% are observed for FeS_2@HTCN/vis and FeS_2@HTCN/H_2O_2 system, respectively. Nevertheless, the degradation rate dramatically increases to nearly 100% in the collaborated effect of FeS_2@HTCN, H_2O_2 and visible light. These results further

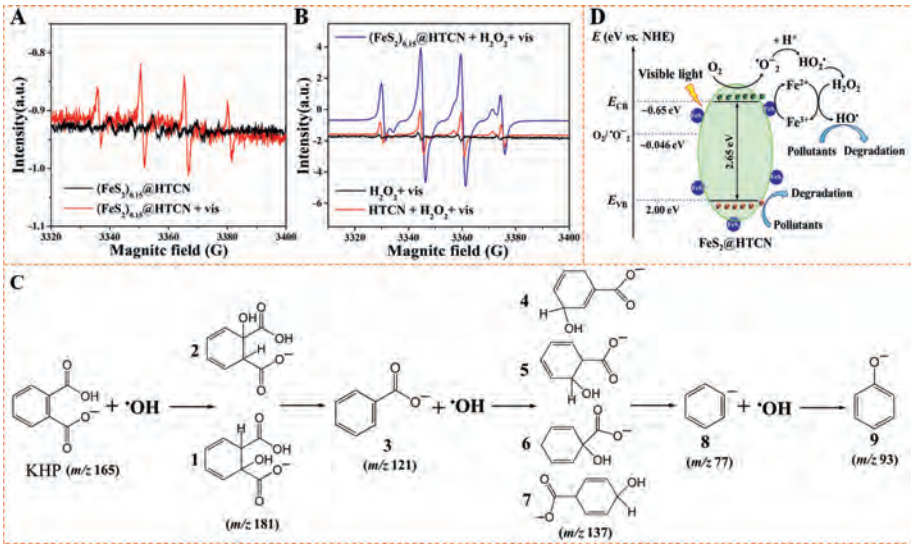

Fig. 4. EPR spectra of EPR spectra of DMPO-HO• adduct formed (A) with $(FeS_2)_{0.15}$@HTCN in the dark and under visible light irradiation, and (B) in the H_2O_2/vis system with different catalysts. (C) Potential photocatalytic degradation pathway of KHP. (D) The schematic illustration of catalytic degradation mechanism.

demonstrate that removal of organic pollutants relies on both Fenton reaction and photocatalytic oxidation. Based on the degradation intermediates found by LC-MS analysis (Fig. S15 in Supporting information), a degradation pathway for KHP is presented in Fig. 4C. The results of COD reduction and TOC analysis infers that further decomposition of these intermediates is effectively proceeded to produce CO_2 and H_2O, suggesting the molecules like KHP can be eventually mineralized in $(FeS_2)_{0.15}$@HTCN/H_2O_2/vis system.

Band structures were measured to explain the generation and migration of photo-excited charge carriers. Based on the results presented in Fig. S16 and Table S4 (Supporting information), a possible degradation mechanism was proposed in Fig. 4D. Although the direct evidence of $^{\bullet}O_2^-$ formation is not observed in EPR tests, the E_{CB} of $(FeS_2)_{0.15}$@HTCN is more negative than the standard redox potential of $O_2/^{\bullet}O_2^-$ (−0.046 eV), however $^{\bullet}O_2^-$ is most probably produced from trapping the photoexcited e^- in the CB by O_2. Then the H_2O_2 can be produced from the dismutation of $^{\bullet}O_2^-$ [44,45], which is conducive to the formation of •OH species. Second, the shortened E_g in $(FeS_2)_{0.15}$@HTCN indicates that the formation of heterojunction can facilitate the separation and transfer of e^- in composite to enhance the circulation of Fe^{2+}/Fe^{3+}. Third, the E_{VB} of $(FeS_2)_{0.15}$@HTCN is less positive than the standard redox potential of $^{\bullet}OH/H_2O$, suggesting that •OH species is produced from the decomposition of H_2O_2. Thus the enhanced •OH generation as well as the reinforced Fe^{2+}/Fe^{3+} circulation should be accountable for the high degradation efficiency of $(FeS_2)_{0.15}$@HTCN catalyzed photo Fenton system.

In conclusion, the molecular self-assembly and molten salt-assisted calcination method were proved to be successful in the synthesis of HTCN. A photo-Fenton catalyst FeS_2@HTCN was prepared by coupling FeS_2 with HTCN via the heterojunction formation, which was proved to be highly effective in the removal of COD for both model compounds as well as real paint wastewater. Comprehensive characterizations demonstrated that the unique structure of HTCN and heterojunction in FeS_2@HTCN are responsible for the improved light absorption ability, enhanced charge carrier migration, suppressed e^-−h^+ recombination and reinforced Fe^{2+}/Fe^{3+} circulation, and increased generation of •OH. A possible degradation mechanism was proposed based on model compound analysis. In view of excellent catalytic efficiency, high stability, good reusability, and considerable economic benefit, the FeS_2@HTCN-based photo-Fenton process is a promising method for industrial wastewater treatment.

Declaration of competing interest

The authors declare that they have no known competing financial interests or personal relationships that could have appeared to influence the work reported in this paper.

Acknowledgments

This work is supported by the Natural National Science Foundation of China (No. 51973083), National First-Class Discipline Program of Food Science and Technology (No. JUFSTR20180301), China Postdoctoral Science Foundation (No. 2019M651688), and Fundamental Research Funds for the Central Universities (No. JUSRP22027). Dr Chan Wang would like to acknowledge the work of Central Laboratory, School of Chemical and Material Engineering, Jiangnan University.

Supplementary materials

Supplementary material associated with this article can be found, in the online version, at doi:10.1016/j.cclet.2021.09.051.

References

[1] R. Mohtashami, J.Q. Shang, J. Clean. Prod. 218 (2019) 335–346.
[2] M.H. Ordouei, A. Elkamel, J. Clean. Prod. 166 (2017) 253–262.
[3] A.A. Zorpas, V.J. Inglezakis, Technol. Soc. 34 (2012) 55–83.
[4] K.Y. Show, M. Ling, H. Guo, D.J. Lee, Bioresour. Technol. 310 (2020) 123376.
[5] D. Güven, O. Hanhan, E.C. Aksoy, G. Insel, E. Çogör, J. Hazard. Mater. 330 (2017) 61–67.
[6] A.D. Barbosa, L.F. da Silva, H.M. de Paula, et al., Water Res. 145 (2018) 153–161.
[7] I.R. Bautitz, R.F.P. Nogueira, Catal. Today 151 (2010) 94–99.
[8] D.L. Zheng, S.L. Pei, S. Geng, L.S. Zhang, J. Nanosci. Nanotechnol. 19 (2019) 5858–5863.
[9] E. López−Loveira, F. Ariganello, M.S. Medina, et al., Environ. Sci. Pollut. Res. 24 (2016) 25634–25644.
[10] N.M. Mahmoodi, S. Khorramfar, Desalin. Water Treat. 52 (2014) 5007–5014.
[11] W.J. Li, Y. Li, D. Ning, et al., New J. Chem. 42 (2018) 29–33.
[12] S.J. Yuan, X.H. Dai, Appl. Catal. B: Environ. 154-155 (2014) 252–258.
[13] S. Xavier, R. Gandhimathi, P.V. Nidheesh, et al., Desalin. Water Treat. 57 (2016) 12832–12841.
[14] Y. Gou, P. Chen, L. Yang, et al., Chemosphere 270 (2021) 129481.
[15] P. Zeng, J.J. Du, Y.H. Song, et al., Environ. Earth Sci. 73 (2015) 4979–4987.
[16] E. Kattel, M. Trapido, N. Dulova, Chem. Eng. J. 304 (2016) 646–654.
[17] W. Miao, Y. Liu, X. Chen, Y.X. Zhao, S. Mao, Carbon 159 (2020) 461–470.

[18] Y. Deng, M. Xing, J. Zhang, Appl. Catal. B: Environ. 211 (2017) 157–166.
[19] X. He, H. Fang, D.J. Gosztola, et al., ACS Appl. Mater. Inter. 11 (2019) 12516–12524.
[20] Y.H. Zhang, F.Z. Lv, T. Wu, et al., J. Sol-Gel Sci. Technol. 59 (2011) 387–391.
[21] S.F. Kang, C.H. Liao, S.T. Po, Chemosphere 41 (2000) 1287–1294.
[22] S.F. Kang, C.H. Liao, H.P. Hung, J. Hazard. Mater. B 65 (1999) 317–333.
[23] J.T. Gao, Y. Wang, S.J. Zhou, W. Lin, Y. Kong, ChemCatChem 9 (2017) 1708–1715.
[24] M.A. Qamar, S. Shahid, M. Javed, Ceram. Int. 46 (2020) 22171–22180.
[25] C.W. Wang, H.F. Zhao, J. Wang, et al., J. Mater. Chem. A 7 (2019) 1451–1458.
[26] B.Q. Wei, C. Wang, Y.M. He, G. X. Ran, Q. J. Song. Compos. Commun. 24 (2021) 100652.
[27] W. Luo, W.Y. Huang, X.Q. Feng, et al., RSC Adv. 10 (2020) 21876–21886.
[28] X. Wang, M. He, Z. Nan, Sep. Purif. Technol. 256 (2021) 117765.
[29] Y.S. Jun, E.Z. Lee, X. Wang, et al., Adv. Funct. Mater. 23 (2013) 3661–3667.
[30] S. Guo, Z.P. Deng, M.X. Li, et al., Angew. Chem. Int. Ed. 55 (2016) 1830–1834.
[31] S. Zhao, Y.W. Zhang, Y.M. Zhou, et al., Carbon 126 (2018) 247–256.
[32] C. Wang, Y. Chen, T. Hu, et al., Nanoscale 11 (2019) 11967–11974.
[33] G.G. Liu, G.X. Zhao, W. Zhou, Y.Y. Liu, H. Pang, Adv. Funct. Mater. 26 (2016) 6822–6829.
[34] F. Yang, D.Z. Liu, Y.X. Li, L.J. Cheng, J.H. Ye, Appl. Catal. B: Environ. 240 (2019) 64–71.
[35] X.Y. Qian, X.Q. Meng, J.W. Sun, et al., ACS Appl. Mater. Inter. 11 (2019) 27226–27232.
[36] S. Zhou, Y. Liu, J.M. Li, et al., Appl. Catal. B: Environ. 158-159 (2014) 20–29.
[37] J. Ye, Y.P. Zang, Q.Y. Wang, et al., J. Energy Chem. 56 (2021) 283–289.
[38] R.G. Morais, N. Rey-Raap, J.L. Figueiredo, M.F.R. Pereira, J. Energy Chem. 50 (2020) 260–270.
[39] C. Cai, Z. Zhang, J Liu, et al., Appl. Catal. B: Environ. 182 (2016) 456–468.
[40] F.A. Barreiro, Y. Kumagai, M. Jonsson, J. Coord. Chem. 71 (2018) 1799–1807.
[41] G. Anirudh, G. Anurag, Chemosphere 193 (2018) 1181–1188.
[42] H. Kusič, N. Koprivanac, A.L. Božič, I. Selanec, J. Hazard. Mater. 136 (2006) 632–644.
[43] S. Xavier, R. Gandhimathi, P.V. Nidheesh, S.T. Ramesh, Desalin. Water Treat. 57 (2016) 12832–12841.
[44] L.Q. Ye, J.Y. Liu, Z. Jiang, T.Y. Peng, L. Zan, Appl. Catal. B: Environ. 142-143 (2013) 1–7.
[45] L. Wang, Y. Chen, B.Y. Chen, J. Yang, J. Hazard. Mater. 404 (2021) 124040.